ResearchGate

See discussions, stats, and author profiles for this publication at: https://www.researchgate.net/publication/258684243

Role of Particle Size and Polymer Length in Rheology of Colloid−Polymer Composites

ARTICLE *in* MACROMOLECULES · DECEMBER 2012

Impact Factor: 5.8 · DOI: 10.1021/ma301184t

CITATIONS
9

READS
35

2 AUTHORS:

Tianying Jiang
3M
7 PUBLICATIONS **26** CITATIONS
SEE PROFILE

Charles Zukoski
University at Buffalo, The State University of N…
208 PUBLICATIONS **8,942** CITATIONS
SEE PROFILE

Available from: Tianying Jiang
Retrieved on: 31 January 2016

Macromolecules

Article

pubs.acs.org/Macromolecules

Role of Particle Size and Polymer Length in Rheology of Colloid–Polymer Composites

Tianying Jiang and Charles F. Zukoski*

Department of Chemical and Biomolecular Engineering, University of Illinois Urbana–Champaign, Urbana, Illinois 61801, United States

Supporting Information

ABSTRACT: The effect of particle size on the flow properties of composite melts is explored. We investigate a system composed of silica particles with diameter D_c = 127–730 nm in unentangled poly(ethylene glycol) of two molecular weights (400 with degree of polymerization ∼9 and 2000 with degree of polymerization of 45). At low concentration, silica particles are stabilized by the adsorbed polymer layer as indicated by intrinsic viscosities slightly larger than the Einstein value of 2.5. Huggins coefficients indicate that at low concentration in PEG400 the particles behave very much like hard spheres, while in PEG2000 the particles experience very weak attractions. At high volume fraction, the absorbed polymer layers begin to interact such that hard-sphere scaling no longer applies to linear and nonlinear rheological responses. In PEG2000, at elevated volume fractions, the particles with stronger attractions experience kinetic arrest with average particle surface separations much larger than the polymer radius of gyration, R_g. We show that the linear rheology, yielding behavior, and shear thickening response of dense composites are varied with R_g/D_c, with volume exclusion glass formation observed at low R_g/D_c and gelation at high R_g/D_c, and with yielding and shear thickening properties changed by R_g and D_c independently. The polymer layers are found to alter the approach to the jamming transition even for R_g/D_c as small as 6×10^{-3}.

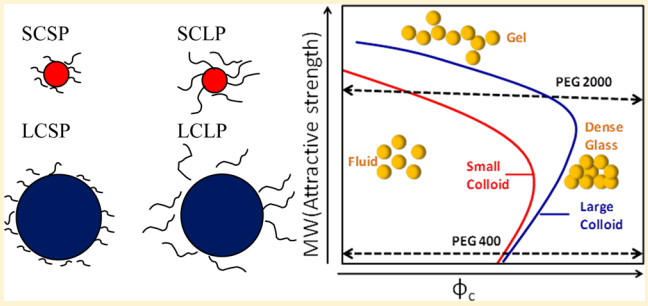

I. INTRODUCTION

The mechanical properties of polymers are often enhanced by addition of submicrometer colloidal particles.[1] Such particle filled polymer melts are referred to as nanocomposite when the particle size is below ∼100 nm in diameter. Particles can enhance elasticity, push the composite glass transition temperature up or down, and can increase or decrease the viscosity of the composite melt.[2,3] Previous studies that focused on the rheology of unentangled polymer nanocomposite melts demonstrated that in miscible systems the rheology of the composite melt is well described as effective hard spheres suspended in a Newtonian continuous phase up to a high packing fractions.[2,4] On the other hand, for the same polymer–particle systems, at fixed particle size when the polymer molecular weight is increased to a value near where the polymer chains entangle, detailed studies of composite microstructure demonstrate the inappropriateness of treating polymer melts as structureless continuum even when the ratio of polymer radius of gyration to the particle diameter, R_g/D_c, is only 0.02.[2]

Here we investigate changes in flow properties in composites of unentangled poly(ethylene glycol) (PEG) with a focus on the effects of silica particle size and high rates of deformation. We are interested in uncovering the effects of particle size and polymer molecular weight on the reinforcing properties of highly filled composites while exploring melt flow properties at shear rates where these composites thicken. In these systems, PEG adsorbs to the particle surface, giving rise to particle and polymer miscibility. The particle's index of refraction is nearly matched to that of the polymer, and charges at the particle surface are eliminated by the low dielectric constant of the polymer melt such that direct interparticle interactions are limited to very weak van der Waals attractions. At low particle volume fractions these systems are thus expected to have rheological behavior similar to that of polymer-coated particles in a Newtonian continuous phase.

When macroscopic surfaces are driven together in a polymer melt where the polymer adsorbs to the particle surface, soft repulsions begin to appear when the surfaces are separated at a distance of less than ∼5–6R_g, with a hard repulsion developing for separations of 2–3R_g.[5,6] In colloid filled polymer melts, the hard particle surfaces alter polymer configurations. These zones of altered configuration begin to interact as the particle volume fraction is raised. As with macroscopic surfaces, when the average surface separation between two particles, h, in units of D_c is estimated as $h/D_c = (\phi_m/\phi_c)^{1/3} - 1$, adsorbed polymer layers begin to interact at $h/R_g < 3.6$ for unentangled polymer and $h/R_g < 6$ for entangled polymer. Here ϕ_c is the volume fraction and ϕ_m is the maximum packing fraction (∼0.64 for

Received: June 11, 2012
Revised: September 19, 2012
Published: December 4, 2012

ACS Publications © 2012 American Chemical Society

spheres). As a result, in addition to chemical details of segment−particle surface interactions, the potential of mean force between particles is expected to be a function of D_c, R_g, and volume fraction just as charge stabilized particles, the interaction between which is a function of D_c, $1/\kappa$ (Debye length), and ϕ_c.[7,8]

For particles suspended in polymer melts to experience soft repulsions mediated by the adsorbed polymer layer, the appropriate attraction strength between polymer segments and particle surface must be achieved. Weak attractions result in depletion attractions that drive the particles to aggregate. Thus, to produce a stable dispersion of particles in a melt, the polymers must experience a net attraction to the particle surface.[9] The polymer reference site interaction model (PRISM) of Schweizer and co-workers has been developed to predict microstructures of polymer and particles in nanocomposite melts.[10] Comparisons of polymer and particle microstructure for low molecular weight unentangled polymer with PRISM predictions show near-quantitative agreement.[11,12] PRISM predicts weak changes to composite microstructure and adsorbed layer thickness with increasing polymer molecular weight.

Contrast matching neutron scattering[13] and rheological studies[14] demonstrate that the adsorbed polymer layer grows in thickness with increasing molecular weight. Indeed, Anderson et al. show that when working with 44 nm silica particles suspended in poly(ethylene glycol) melts with molecular weights of 400−20 000, the particle's intrinsic viscosity increased in a manner consistent with an effective hard core diameter of $D_c(1 + 2.8R_g/D_c)$.[14] Anderson et al. reported that this increase in effective particle size with molecular weight is accompanied by a decrease in colloidal stability indicative of a weakening of repulsions or the introduction of weak interparticle attractions. However, for low molecular weight (MW < 1000), the effective hard-sphere model captures the linear viscoelastic rheology until particles are brought to a volume fraction where $h/D_c \sim 3.6R_g/D_c$. Increases in adsorbed polymer layer thickness are associated with greater structure in colloidal suspensions. There is thus some confusion as to success of PRISM for low molecular weight polymer composites as well as the failure of PRISM at higher molecular weights based on the nature of the absorbed polymer layer and how it influences the potential of mean force felt by the particles. These observations of silica in PEG melts augment earlier studies of polybutylene melts filled with polystyrene spheres[15] and suggest that nonequilibrium polymer configurations become increasingly dominant as polymer molecular weight grows.

Here nonequilibrium configurations are associated with the inability of adsorbed polymer segments to rapidly exchange with those in the bulk such that polymer configurations near the particle surface cannot relax into an equilibrium state over reasonable time scales. The increased segment residence time at the particle surface alters particle and polymer microstructures.[13] In studies of composites made of 44 nm silica in PEG for molecular weights above 3000, the proximity of the surfaces was found to introduce greater entanglement at volume fractions where $h/D_c < 6R_g/D_c$. The interaction of the adsorbed polymer layers at these average surface spacing does not lead to particle aggregation, but increasing polymer MW does result in kinetic arrest of the particles at $\phi_c \sim 0.30$ and the composites displaying brittle fracture. The gel transition observed in these systems is not well described as a glass transition of effective hard spheres.

A variety of previous studies have explored the role of soft repulsions on linear and nonlinear suspension rheology. For example, the effects of particle size and polymer induced interaction potentials on rheological properties and microstructure of charged polymer colloids (with varying ionic strength), particles with grafted polymers (fixed graft size and variable particle size[16]), and microgel systems and particles with the core−shell microstructures have been extensively reported.[17−20] Often, these studies analyze experimental observations starting models where the adsorbed or grafted polymers starts define an effective hard core volume fraction that accounts for the increased excluded volume introduced by the adsorbed or grafted polymer layers.

Consistently, as volume fraction is raised, there is a transition from a state where a zero shear rate viscosity can be measured to a state the suspensions shear thinned in all measurable shear rates, $\dot{\gamma}$. Often volume fractions are reached where the suspensions show a dynamic yield stress where the stress is very weakly dependent on $\dot{\gamma}$ followed at high shear rates by the approach of a high shear rate terminal viscosity. At effective volume fractions where the yield stress plateau develops, the linear elastic storage modulus, G', displays a high-frequency plateau while the linear loss modulus, G'', develops a minimum indicating a separation of relaxation time scales. These features are consistent with the onset of glassy behavior as predicted by mode coupling theory (MCT).[17] However, at effective volume fractions where absorbed polymer layers begin to interact, the deformability of adsorbed or grafted layers dominate the flow,[20] demonstrating the need for care in interpreting the flow properties at high volume fraction and high stresses.

Working with a range of particle sizes enables us to explore a broad range of shear rates. The particles are Brownian and for the Newtonian polymer melts studied here, the diffusivity can be written as $D_0 = k_BT/3\pi\eta_pD_c$. Here η_p is the viscosity of solvent and k_BT is product of the Boltzmann parameter and absolute temperature. Typically shear thickening is associated with high applied stresses where hydrodynamic interactions dominate the suspension microstructure. This occurs where the rate of shear is larger than the rate of diffusion. This ratio of rates is characterized by the Peclet number, $Pe = 3\pi\eta_p\dot{\gamma}D_c^3/4k_BT$, and thickening is typically observed when $Pe > 10$.[21] Thickening becomes noticeable as the volume fraction increases and initially is observed as a logarithmic increase viscosity with shear rate. As the volume fraction approaches close packing, the viscosity undergoes a discontinuous increase as shear rate is increased.

If thermally active particles are suspended in a Newtonian continuum and experience only hard core interactions, dimensional analysis suggests that for a given volume fraction shear thickening will be observed at a universal value of Pe.[21] As a result, the absolute shear stress at the onset of shear thickening satisfies $\tau_c \propto D_c^{-3}$. When interactions other than those of volume exclusion are operational, the size dependence of τ_c will change. For example, for particles experiencing short-range, screened electrostatic repulsions satisfy $\tau_c \propto D_c^{-2.7}$. Similar results have been observed with particles experiencing soft repulsions that demonstrate the sensitivity of shear thickening to the hydrodynamic permeability of polymer coat.[16,22] Attractions are known to delay thickening to larger stresses[23] while soft polymer layers are known to weaken the onset of thickening.[22] Little has been reported for shear

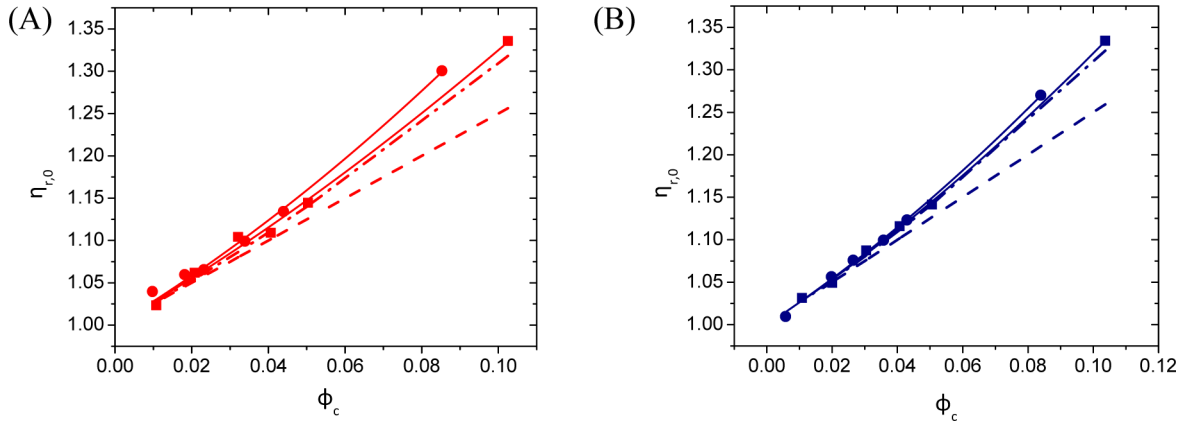

Figure 1. Measurement of the zero shear viscosity of PEG400 (square) and PEG2000 (circle) as a function of ϕ_c for (A) small particles and (B) large particles, with Einstein's equation (dashed line) and Einstein's equation with second term (dot-dashed line) included and fitting curve to eq 1 (solid line).

thickening in nanocomposite melts where, as discussed above, the effects of particle size, interactions of absorbed polymer layers, and changes to the potential of mean force due to nonequilibirum polymer configurations become important.

Here we focus on four different colloid−polymer composites composed of two different silica particle sizes (D_c = 127 nm referred to as small particles and D_c = 612 nm referred to as large particles) and two different polymer molecular weights (poly(ethylene glycol) with molecular weight equaling to 400 and 2000 where the molecular weight for entanglement is ∼4000).[14] In section II we discuss how we create our composites and characterize composite rheology under steady shear and in linear and nonlinear oscillatory rheometry.

In section III we discuss our results with careful attention to the magnitudes moduli, volume fraction dependencies of characteristic frequencies extracted from linear elastic studies, and yielding behavior with a particular focus on flow curves and the stress at the onset of thickening. We show that there are three effects altering composite mechanics at high volume fractions with increasing polymer molecular weight and increasing particle size. First, we show that the potential of mean force experienced by the particles suspended in polymer melts is altered by particle size, and this effect is enhanced in high-MW polymer melts. Second, as polymer molecular weight grows—even below the entanglement molecular weight—particles experience weak attractions that extend beyond the extent of bound polymer layers. We attribute these attractions to very slow exchange of absorbed polymer segments with those in the bulk. This gives rise to the effective particle surface becoming chemically similar to the bulk such that the enthalpy of exchange of a segment from bulk to the effective particle surface drops, resulting in a depletion attraction. Third, as the volume fraction is raised such that h/R_g is of order unity, interactions of the polymer layers begin to dominate flow properties. Finally, we report that in the composites formed of the low molecular weight polymer hard sphere scaling is not observed at shear thickening and that shear thickening is considerably weakened as polymer molecular weight is increased.

II. EXPERIMENTAL METHODS

A. Sample Preparation. Monodisperse silica particles are synthesized by method that is developed by Stober[24] and extended by Bogush et al.[25] Two different sizes are prepared with D_l = 612 ± 20 nm (referred to as large particles) and D_s = 127 ± 7 nm (referred to as small particles) which will be mainly discussed below. In addition, two more particle sizes are included in shear thickening behavior study for low molecular weight which are 730 ± 8 and 213 ± 9 nm particles. The product particles are suspended in ethanol solution containing water and ammonia hydroxide. The resulting suspension is concentrated to a mass fraction ∼0.20 by heating up the suspension to evaporate the solvent and drive off the ammonia. Following previous studies,[2] we chose to work with poly(ethylene glycol) with MW ∼ 400 (MW: 380−420, PEG400, low molecular polymer) at T = 25 °C and MW ∼ 2000 (MW: 1900−2200, PEG2000, high molecular polymer) at T = 75 °C as the polymer melts. PEG400 is a Newtonian fluid with viscosity ∼0.10 Pa·s at T = 25 °C. PEG2000 is also a Newtonian fluid at the condition we study with viscosity ∼0.10 Pa·s at T = 75 °C.

Concentrated silica particle suspensions are mixed with PEG and the resulting suspensions are placed into a vacuum oven with temperature kept above T_m of PEG to remove ethanol. Below we refer to the four different sets of composites separately as SCSP (small colloid in short polymer), LCSP (large colloid in short polymer), SCLP (small colloid in long polymer), and LCLP (large colloid in long polymer). To determine the volume fraction ϕ_c of particle with mass fraction X_c < 0.50, the equation $\phi_c = (\rho_T/\rho_c)X_c$ is used, where ρ_T and ρ_c are the density of the filled composites and pure polymer melts. The composite density, ρ_T, is determined using a Mettler/KEM DA-100 density meter for low molecular weight polymer (PEG400). The particle density was measured in previous studies to be ρ_c = 1.6 g/cm^3.[2] The results are quite consistent for large and small particles for the same mass fraction samples. For X_c > 0.50, the composite viscosity was too high to be measured in the density meter and volume fraction was determined by extrapolating the plot in the ϕ_c−X_c panel. Previous study has confirmed a similar density of composites independent of polymer molecular weight,[14] so we would use the same volume fraction here for SCLP and LCLP at same mass fractions.

B. Rheology. Rheology experiment is carried out with a C-VOR Bohlin rheometer where a cone and plate geometry is used. The cone diameter is 20 mm with a 4° angle. Here the temperature is kept at 25 °C for PEG400 and 75 °C for PEG2000 to keep the similar matrix viscosity high enough (η_p = 0.10 Pa·s) to make sure of studying in a high dimensionless frequency range ($\omega^* = 3\pi\eta_p\omega D_c^3/k_BT$) and high dimensionless shear rate range ($Pe = 3\pi\eta_p\dot{\gamma}D_c^3/4k_BT$) to observe shear thickening in the measurement window which will be discussed below.

Oscillatory stress is used to measure elastic modulus G' and viscous modulus G'' as a function of frequency ω in the frequency sweep experiment with strain γ = 0.01 held constant to make sure of searching in a linear region, and G' and G'' are measured by varying shear stress/strain at fixed frequency ω = 0.1 Hz to study the nonlinear rheology and yielding behavior. Moreover, continuous stress is applied in the viscometry measurement to study the viscosity as a function of

dx.doi.org/10.1021/ma301184t | Macromolecules 2012, 45, 9791−9803

Table 1. Fitting Parameters for Zero Shear Viscosity at Low Concentration

	D_c = 127 nm				D_c = 612 nm			
	k	H	δ (nm)	R_g/D_c	k	H	δ (nm)	R_g/D_c
PEG 400 (R_g = 0.8 nm)	1.06 ± 0.08	5.4 ± 2.0	1.2	6×10^{-3}	1.01 ± 0.04	6.5 ± 1.0	1.0	1.3×10^{-3}
PEG2000 (R_g = 1.9 nm)	1.09 ± 0.08	7.6 ± 1.1	1.9	1.5×10^{-2}	1.02 ± 0.04	7.6 ± 1.3	2.0	3.1×10^{-3}

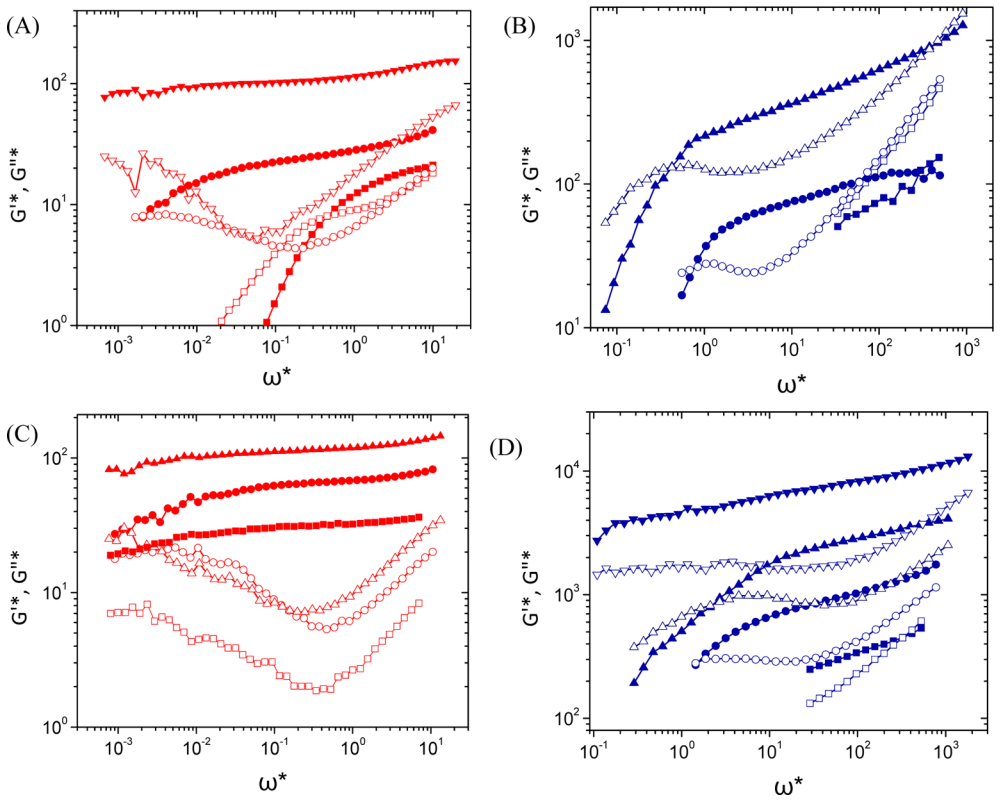

Figure 2. Linear G'^* (closed symbols) and G''^* (open symbols) for (A) SCSP at ϕ_c = 0.511 (■, □), 0.534 (●, ○), and 0.604 (▼, ▽); (B) LCSP at ϕ_c = 0.580 (■, □), 0.604 (●, ○), and 0.629 (▲, △); (C) SCLP at ϕ_c = 0.369 (■, □), 0.438 (●, ○) and 0.479 (▲, △); and (D) LCLP at ϕ_c = 0.549 (■, □), 0.570 (●, ○), 0.592 (▲, △), and 0.615 (▼, ▽).

applied shear stress or shear rate to understand the shear thickening behavior. Preshear has been applied and 1 min recovery time has been allowed before each measurement. We found that the samples recovered their properties within the time frame of switching shear stresses. The measurements were found to be reproducible with the samples showing no thixotropy and flow properties being independent of shear history.

III. RESULTS AND DISCUSSION

A. Low Concentration Viscosity. In Figure 1, the relative zero shear viscosity $\eta_{r,0} = \eta_0/\eta_p$ is plotted as a function of silica particle volume fraction, where η_0 is the viscosity in the low shear rate region and η_p is the polymer matrix viscosity (η_p = 0.10 Pa·s for PEG400 at T = 25 °C and for PEG2000 at T = 75 °C), and the resulting low volume fraction data are fit to

$$\eta_{r,0} = 1 + 2.5k\phi_c + H(k\phi_c)^2 \quad (1)$$

Here $k = \phi_{eff}/\phi_c$ with ϕ_{eff} standing for the effective hard sphere volume fraction and H is interaction coefficient which should be 5.9 for hard sphere interaction.[26] The fitting results are also included in Table 1.

Within experimental uncertainty, when suspended in PEG 400, both large and small particles behave essentially like hard spheres with single particles dissipating energy as if they have a slightly larger core size. An effective particle size can be calculated from k assuming that single particles dissipate energy under shear as if they were composed with a hard core surrounded by an immobilized polymer layer with thickness δ at the outer edge of which the nonslip boundary condition holds. Under these conditions, $k = \phi_{eff}/\phi_c = (D_{eff}/D_c)^3 = (1 + 2\delta/D_c)^3$. We tabulate the values of δ in Table 1. For PEG2000, k is larger than for PEG400, showing that the steric layer thickness is independent of the particle size, but increases proportionally with the square root of the polymer polymerization degree in agreement with previous work, where steric layer thickness is found to be proportional to R_g ($R_g \propto \sqrt{N}$ with N representing the polymerization degree) for PEG with MW in the range 400−20 000.[14] The values in Table 1 are smaller than the values reported for 44 nm diameter silica particles reported previously,[14] which may reflect the effects of surface curvature. Also for PEG2000, H is increased slightly for both large and small particles further away from 5.9, denoting enhanced pair interactions. However, H lies close to the hard sphere value of 5.9, showing that the interaction is small for both PEG400 and PEG2000.

B. Linear Rheology. At elevated volume fractions, the linear elastic properties of these composites vary dramatically with particle size and polymer molecular weight. In Figure 2, we

dx.doi.org/10.1021/ma301184t | Macromolecules 2012, 45, 9791−9803

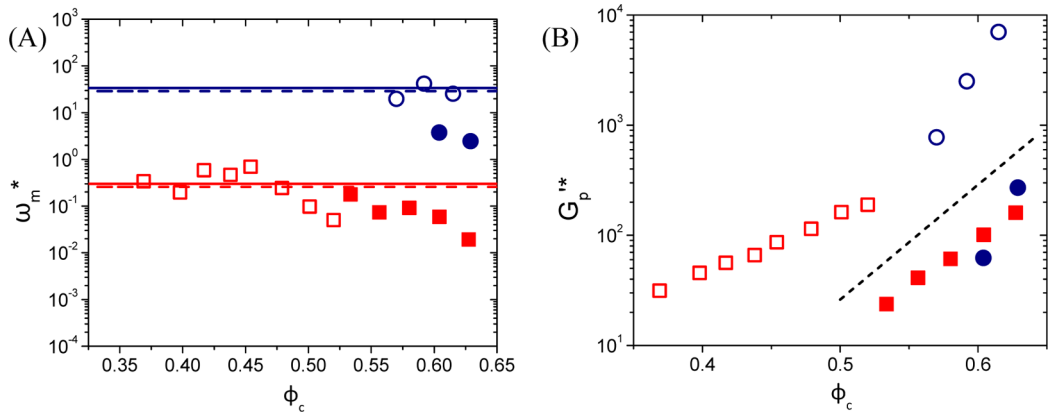

Figure 3. Dimensionless frequency ω_m^* (A) and dimensionless elastic moduli $G_p'^*$ (B) at the local minimum of G''^* point plot with volume fraction for SCSP (■), LCSP (●), SCLP (□), and LCLP (○). The solid line (red for SCSP, blue for LCSP) and dashed line (red for SCLP, blue for LCLP) in (A) are dimensionless frequencies for f = 0.1 Hz. The dashed line in (B) is prediction of Kobelev et al.[30]

present the linear elastic moduli and viscous moduli as a function of frequency for representative volume fractions of the four sets of composites. Here the dimensionless parameters are obtained as follows: $G'^* = G'D_c^3/k_BT$, $G''^* = G''D_c^3/k_BT$, and $\omega^* = \omega D_c^3/D_0$, where G', G'', and ω are the elastic modulus, viscous modulus, and angular frequency ($\omega = 2\pi f$ with f representing frequency in unit of Hz), and D_0 is the dilute particle diffusion coefficient.

At low frequencies the composites enter a low-frequency terminal region where both G'^* and G''^* increase as power law functions of ω^* with exponents of 2 and 1, respectively, below a crossing point ω_{x1}^*, where $G'^* = G''^* = G_{x1}^*$.[27] For the data shown in Figure 2, the terminal region is only observed with LCSP, while for the other three sets of data, the terminal region is entered at frequencies lower than could be probed. At even higher frequencies, there is a second crossing point at ω_{x2}^*, where $G''^* > G'^*$. As the volume fraction increases, a minimum develops in G'' at ω_m and G' develops a "rubbery" plateau, $G_p' = G'(\omega_m)$.

In the terminal region at low frequencies, the viscous nature of the composite is probed with composite's zero shear rate viscosity given by G''/ω. The crossover frequency ω_{x1}^* characterizes the rate particles can diffuse out of nearest-neighbor cages such that the inverse of ω_{x1}^* is comparable to the α-relaxation time of colloidal glasses.[28,29] At frequencies between ω_{x1}^* and ω_{x2}^*, the sample is deformed at rates where particles cannot exchange nearest neighbors but at rates slower than the time it takes particles to explore the nearest-neighbor cage. For frequencies greater than ω_{x2}^*, the deformation rate becomes larger than the short time rate of particle diffusion within their cage, particle motion is increasingly frozen, and the suspension responds with a high-frequency viscosity.[27]

As shown in Figure 2, due to fixed instrumental frequency range and a substantial change in particle volume, the range of dimensionless frequencies covered by the experiments for large and small particles are substantially different. A consequence is that we cannot probe the low frequency region for large particle composites, and we cannot probe deeply into the high frequency region for small particle composites. In addition, we note that the range of dimensionless moduli measured is substantially larger for the large particles than for the small particles. Despite the large dimensionless moduli reported, the absolute moduli for the large particles are small, and thus we can only report reliable measurements at the largest volume fractions studied.

As mentioned above, values of the $1/\omega_{x1}$ (or the frequency at the maximum in G'') are often taken as characterizing the α-relaxation time for particles diffusing out of nearest-neighbor cages[4,28] For near hard sphere interactions, the α-relaxation frequency decreases with increasing volume fraction as $(\phi_g - \phi_c)^{-\alpha}$ with $\phi_g \sim 0.58$ up to a critical volume fraction above which this critical scaling is no longer observed, and the α-relaxation time increases more slowly with volume fraction.[4] The deviation from the critical scaling is taken as an indication that the system has entered an activated relaxation zone where relaxation times will diverge only at random close packing. In the activated glassy transport model of Schweizer and co-workers, the magnitude of relaxation time in the activated region is set by the height of a dynamical potential which is determined in a self-consistent manner from the equilibrium microstructure and D_0 while the magnitude of the elastic modulus is set by the curvature of the dynamical potential at its minimum.

We note that $\omega_{x1}^* < 10^{-3}$ for SCSP and for LCSP $10^{-1} < \omega_{x1}^* < 10^0$ for similar range of volume fractions and that there is a greater characteristic frequency as determined by ω_{x1}^* and ω_m^* for the small particles than the large particles. Interpreted in terms of the activated transport model, this suggests that, at the same volume fraction, the confining potential for the large particles has a lower barrier across which the particles must diffuse to exchange nearest neighbors than is experienced by the small particles. Moving to higher MW, we see that ω_{x1}^* for SCLP is less than 5×10^{-4} for all volume fractions greater than 0.39, indicating greatly reduced rates of long-range diffusion are created by suspending the small particles in higher molecular weight melts. On the other hand, ω_{x1}^* for LCLP are of the same order as LCSP showing that the barrier to diffusion is approximately the same at low and high molecular weights, clearly indicating that effects of absorbing polymer are enhanced as the average spacing between the particles shrinks relative to the polymer's radius of gyration.

In the frequency range between ω_{x1}^* and ω_{x2}^*, the particles remain diffusive but cannot exchange nearest neighbors. The separation of time scales for long-range and short-range diffusion are classic indicators of glass or gel formation. All the composites studied here show this state transition. In Figure 3, we present volume fraction dependencies of ω_m^*,and $G_p'^*$

along with the prediction of Kobelev et al. for hard sphere glasses.[30] The horizontal lines in Figure 3A are dimensionless frequency ω^* for f = 0.1 Hz for the four different sets of composites where we ran stress sweep experiments discussed in the following subsection.

The frequency at the minimum in G'', ω_m, is often taken as a surrogate for the β relaxation time—the time it takes particles to explore nearest-neighbor cages.[4] With this interpretation in mind we see in Figure 3A that the large particles have considerable greater short time diffusivities than small particles when suspended in both low and high molecular weight polymers. We note that we have chosen temperatures such that the viscosity of the PEG400 melt is the same as the PEG2000 such that the shifts in ω_m^* can be made at fixed matrix viscosity η_p. In this case, the self-diffusivity of the particles in the two molecular weight melts is expected to be similar. We note that ω_m^* appears to be a weak function of polymer molecular weight once particle size is fixed. This suggests that despite evidence of greater attractions between particles with increased molecular weights, particle mobility within cages set by nearest neighbors is weakly dependent on polymer molecular weight.

While the changes in ω_{x1} and ω_m are associated with changes to the dynamical potential barrier to diffusion,[31] changes in $G_p'^*$ are associated with probing the curvature of the dynamical potential barrier and its minimum and are argued to have a form $(G'D_c^3)/(k_BT) = 0.58\phi(D_c^2/r_{loc}^2)$,[32] where r_{loc} is the localization length or a measure of the range of local particle motion when trapped within nearest-neighbor cages. When particle−particle attractions are increased, r_{loc} is decreased, resulting in larger elasticity.

In Figure 3B, $G_p'^*$ is essentially the same for SCSP and LCSP with volume fraction dependence captured well by the volume fraction dependence of predicted zero stress dimensionless elastic modulus G'^*: $G'^* = (1.6 \times 10^{-4})e^{26\phi}$ for hard spheres.[30] These results are consistent with the low volume fraction viscosity measures suggesting nearly hard sphere behavior for low molecular weight suspending media[4] and suggest that r_{loc}/D_c is similar for small and large particles in PEG400. We note substantial differences in ω_{x1}^* values for these samples, suggesting that the barrier height for activated diffusion is larger for the small particles. We note that theoretical studies suggest that for hard particles there is a tight linkage between the barrier height, F_B, and the localization length with $F_B \sim r_{loc}^{-1}$,[31] suggesting that elasticities and diffusion times should be inversely correlated. We expect the diffusion times to scale as $\exp(F_B/k_BT)$ such that an increase in modulus will track a rapid drop in ω_{x1}^*. That we do not observe this coupling as we change particle size suggests we are not working with volume exclusion potentials of mean force.

The limiting high frequency behavior of the elastic modulus of colloidal suspensions has been explored by Lionberger and Russel, who show that at high frequencies for no slip boundary conditions $G'^* \sim \omega^{*1/2}$ while for slip boundary conditions G'^* is independent of strain frequency.[33] We note a tendency toward slip boundary conditions as particle size decreases for PEG400.

When polymer MW is increased to 2000, $G_p'^*$ increases tremendously for both large particles and small particles. For SCLP, samples become solid-like when ϕ_c is as low as 0.37, where h/R_g = 13. Because of this average particle separation being approximately twice that where we expect adsorbed polymer layers interact, we conclude that the jump in modulus cannot be explained by repulsive interactions and that these systems form colloidal gels due to attractions. This effect is also seen in the increase of $G_p'^*$ for large particles in moving from small polymer to large polymer melts.

The volume fractions of the large particle composites studied here are well above that where small hard particles display glassy behavior. However, these systems show limited separation at time scales in frequency sweeps and, as discussed below, have a very weak dynamic yield stress plateau in continuous shear studies. This may be attributed to these particles experiencing a weak attraction such that the system lies in a re-entrant glassy region where attractions melt the glass.

These results indicate that particles feel stronger attractions in PEG2000 than in PEG400. Independent of molecular weight, PEG adsorbs strongly to the particle surface.[13] Thus, these attractions are between polymer-coated surfaces. Within the context of a PRISM framework, the primary variable controlling composite microstructure and mechanics is the exchange enthalpy of moving a polymer segment from the bulk to the particle surface, ε_{pc}. If ε_{pc} is small, polymer does not adsorb and depletion attractions develop. Only when ε_{pc} is sufficiently large will thermodynamically stable layers form and the particles and polymer become miscible.[34] Here we have a system where the polymer adsorbs and generates miscible composites. However, the particles are also seen to experience attractions. We believe this is due to nonequilibrium adsorption of polymers arising from increasing number of absorbed polymer segments per chain as polymer molecular weight increases. The increased number of binding segments per chain will reduce the ability of the adsorbed polymers to reach equilibrium with polymer segments in the bulk. As a result, from the perspective of a polymer segment in the bulk, the surface will look as it is composed of PEG segments resulting in a decrease in effective ε_{pc}. Thus, while the exchange enthalpy is sufficient to create a stable polymer layer at each particle surface, because polymers cannot exchange freely with those in the bulk, a weak depletion attraction develops as a result of a drop in the effective ε_{pc}.

From the studies of the linear rheology of these composite melts, we draw two conclusions: (1) As ϕ_c increases, gels or glasses are formed. The high volume fractions where the separation of time scales occurs (for all but SCLP) suggest the systems experience volume exclusion and weak attractions. (2) The differences in ω_m^* for SCSP and LCSP denotes that composite dynamics are controlled by details of interactions while the magnitudes and volume fraction dependencies of G_p^* for these two samples suggest hard sphere behavior. When increasing the MW of polymer, the jump in G_p^* indicates that attractions are introduced.

Having established general features of the polymer induced particle interactions, below we explore the effects of polymer induced attractions on the nonlinear rheology of the composites and changes to the flow properties when the composites are subjected to continuous shear.

C. Nonlinear Rheology and Yielding Behavior. In many reports of suspension dynamics, yielding is investigated by subjecting suspensions to a fixed strain frequency and an increasing maximum strain. At high volume fractions the G'^* is seen to decay while G''^* passes through a maximum and crosses G'^* at a specific strain and stress amplitude. These strains and stresses are typically taken as characterizing yield stress and strain of the suspension. As discussed above and shown in Figure 2, as ω^* is increased above $\sim 10^1-10^2$, ω_{x2}^* is

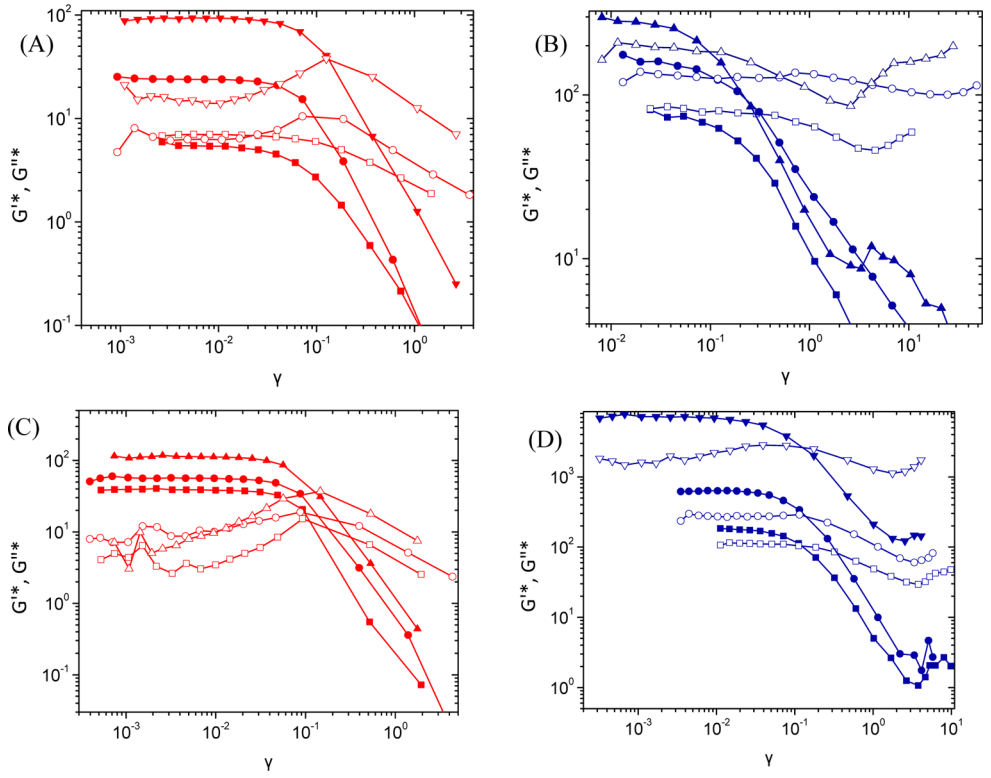

Figure 4. Stress sweep experiment results for $f = 0.1$ Hz with G'^* (closed symbols) and G''^* (open symbols) plot with strain for (A) SCSP at ϕ_c = 0.511 (■, □), 0.534 (●, ○) and 0.604 (▼, ▽); (B) LCSP at ϕ_c = 0.580 (■, □), 0.604 (●, ○), and 0.629 (▲, △); (C) SCLP at ϕ_c = 0.398 (■, □), 0.438 (●, ○), and 0.479 (▲, △); and (D) LCLP at ϕ_c = 0.549 (■, □), 0.570 (●, ○), and 0.615 (▼, ▽).

approached. At these frequencies, for all strains—even in the linear response region $G''^* > G'^*$—this standard method of characterizing yield stresses becomes difficult to interpret. This is of particular concern in studies where particle size is varied as increasing D_c increases ω^* rapidly, driving the sample characterization toward ω_{x2}^* and making it difficult to compare flow properties between materials at the same volume fraction containing particles of different sizes. Here we propose to use a frequency near ω_m^* for amplitude sweeps as a means of characterizing yielding behavior as particle size is varied.

As shown in Figure 3A, $f = 0.1$ Hz is near the frequency ω_m where the minimum of G''^* is detected and rubbery plateau of G'^* is observed. We use this frequency to investigate yielding. By choosing a frequency near ω_m^*, we are looking at yielding at strain frequencies where the particles are trapped in cages. Therefore, we are thus characterizing the nonlinear deformation behavior by increasing the maximum strain at a frequency within a range that exceeds the rate the particles can exchange nearest neighbors and below a frequency where the particles do not respond to flow. As a result, particles have insufficient time to escape from the dynamical arrest state at low strain magnitude but ample time to explore nearest-neighbor cages during a strain cycle.

Results of these amplitude sweeps are shown in Figure 4 where in large strain limit, for the 127 nm particles in both polymers, the moduli decrease $G'^* \propto \gamma^{-2}$, $G''^* \propto \gamma^{-0.6}$ ($\phi_c \geq$ 0.534 for SCSP and $\phi_c \geq 0.398$ for SCLP). For the 612 nm particles in the low molecular weight polymer, $G'^* \propto \gamma^{-1}$ ($\phi_c \geq$ 0.580). When suspended in PEG2000, the large particles have moduli that decay as $G'^* \propto \gamma^{-1.6}$ ($0.504 \leq \phi_c \leq 0.592$) in the large amplitude limit. Here γ is the shear strain. For LCSP (Figure 4B) and LCLP (Figure 4D), the large strain behavior of G''^* is complicated by the onset of strain thickening, where the G''^* is decreased first and then increased in the large γ magnitude limit. To understand this phenomenon better, continuous shear is applied which will be discussed in the next subsection. All these modulus behaviors at large shear strain are summarized in Table 2.

Table 2. Summary of Modulus Behavior at Large Shear Strain

	SCSP	LCSP	SCLP	LCLP
ϕ_c range	$\phi_c \geq 0.534$	$\phi_c \geq 0.580$	$\phi_c \geq 0.398$	$0.504 \leq \phi_c \leq 0.592$
G'^*	$G'^* \propto \gamma^{-2}$	$G'^* \propto \gamma^{-1}$	$G'^* \propto \gamma^{-2}$	$G'^* \propto \gamma^{-1.6}$
G''^*	$G''^* \propto \gamma^{-0.6}$	thickening	$G''^* \propto \gamma^{-0.6}$	thickening

Kobelev and Schweizer extended the activated transport model to predict an absolute yield stress where the applied stress eliminates thermodynamical barrier limiting diffusional exchange of nearest neighbors. In previous studies this has been associated with the stress (strain) in amplitude sweeps where $G'^* = G''^* = G_x^*$.[30] In Figure 5, we present τ_x^* ($\tau_x^* = \tau_x D_c^3/k_BT$), G_x^*, and γ_x which represent a measure of the absolute yield stress, the elasticity at the yield stress, and the strain at the yield stress, respectively.

The trends with change in particle size and molecular weight observed in G_p^* are duplicated in Figures 5A and 5B for τ_x^* and G_x^*. For both large particles and small particles, increasing polymer MW results in increases in stress τ_x^* and elasticity G_x^* at yield point, consistent with the presence of attractions. We note that G_x^* are larger for LCSP than SCSP. We attribute this

dx.doi.org/10.1021/ma301184t | Macromolecules 2012, 45, 9791−9803

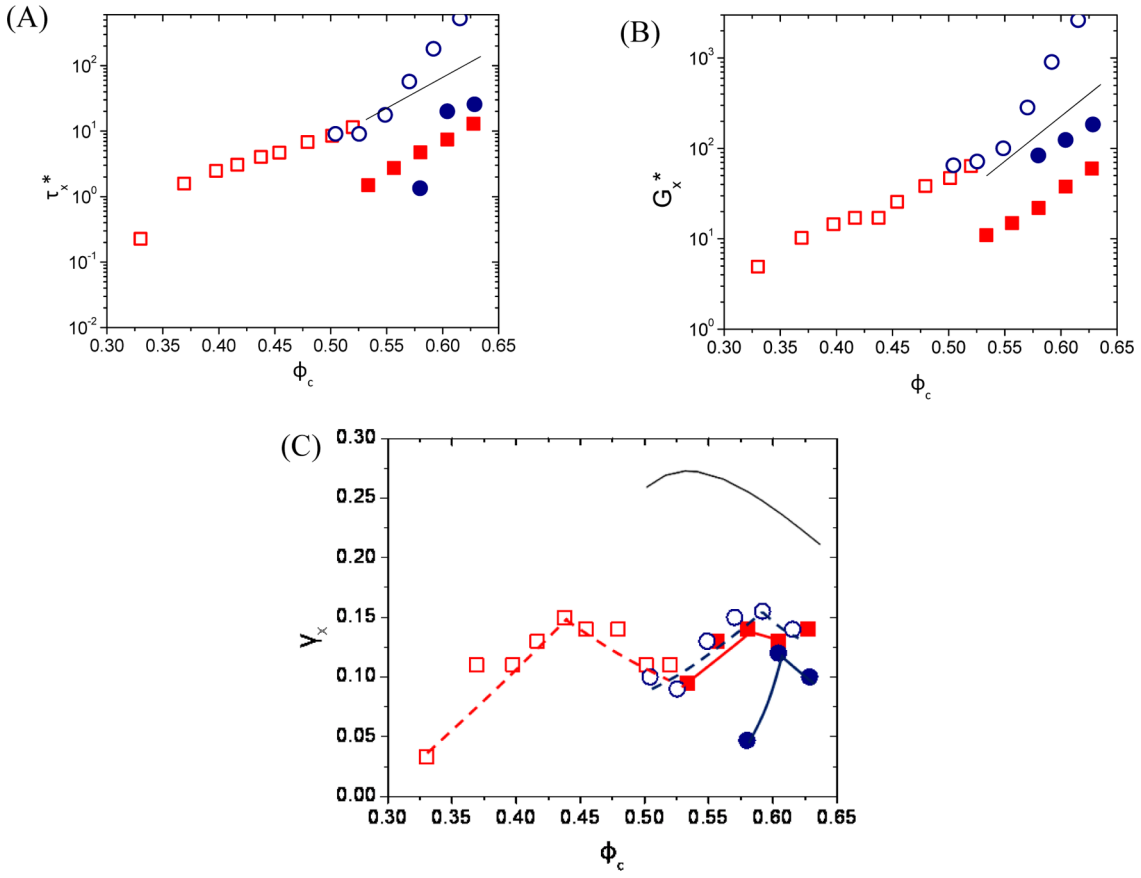

Figure 5. (A) Dimensionless stress τ_x^*, (B) dimensionless elasticity G_x^*, and (C) strain γ_x at the cross point where $G'^* = G''^* = G_x^*$ plot with volume fraction for SCSP (■), LCSP (●), SCLP (□), and LCLP (○). The curves (red solid for SCSP, blue solid for LCSP, red dashed for SCLP, and blue dashed for LCLP) in (C) are used to guide eyes for the peak in γ_x, and the black solid lines are predictions by Kobelev et al.[30]

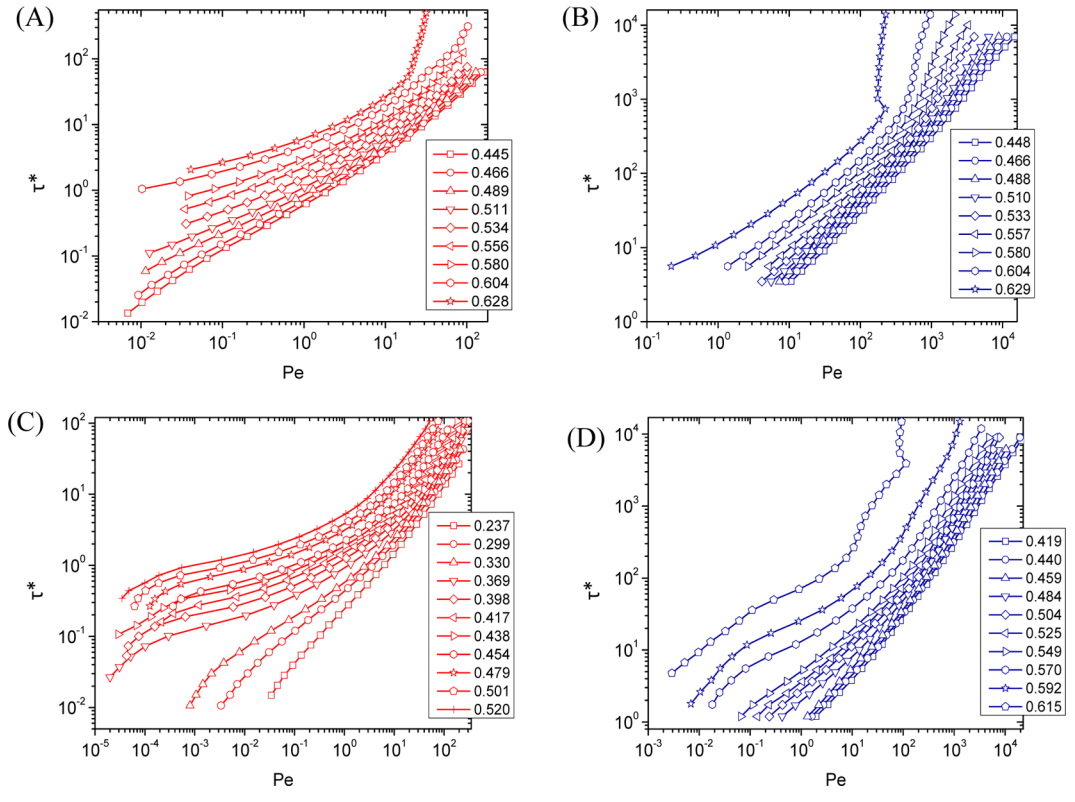

Figure 6. Flow curves for (A) SCSP, (B) LCSP, (C) SCLP, and (D) LCLP.

dx.doi.org/10.1021/ma301184t | *Macromolecules* 2012, 45, 9791−9803

to the larger dimensionless frequency of deformation which pushes G''^* closer to G'^*.

D. Flow Curves and Shear Thickening. The response of the composite melts to continuous shear is presented in Figure 6, where we present the dimensionless stress τ^* as a function of Pe, where $\tau^* = \tau D_c^3/8k_BT$ (where τ is the stress). These composite melts show general flow features expected for concentrated colloidal suspensions: (i) at low Pe and low volume fractions, a terminal region can be observed where in this double-logarithmic plot, the slope of the curve d log(τ)/d log($\dot{\gamma}$) has a value of unity, and the composite melts show a zero shear rate viscosity. (ii) As volume fraction increases the composite melts shear thin at a volume fraction dependent value of $Pe = Pe_1$. As the volume fraction increases, the stress begins to develop a plateau where p = d log(τ)/d log($\dot{\gamma}$) takes on a value $\ll 1$ for an extended Pe region. For the SCLP composites, at the highest volume fractions studied, p approaches zero, indicating the composite melt is showing a dynamic yield stress. (iii) Above a second characteristic volume fraction dependent value of $Pe = Pe_2$, a high shear rate terminal behavior is approached where p again approaches unity. (iv) Pe_2 is weakly dependent on volume fraction while Pe_1 decreases with increasing volume fraction as the dynamic yield stress plateau becomes more prominent. (v) At sufficiently high volume fractions shear thickening occurs at Pe_3 above which the slope $p > 1$. While Pe_3 is a function of volume fraction, the stress at thickening, τ_c^*, is a weak function of volume fraction. We note that these features are those expected of dense suspensions of stable particles suspended in low molecular weight solvents.[16] One thing to note here is that for the highest ϕ_c samples of LCSP and LCLP a double yielding phenomenon is observed for LCSP. This first continuous thickening with smooth change of slope p is explained as a result of hydrocluster formation as other samples; the second discontinuous thickening with sharp change of slope p is attributed to jamming which is only observed at very high ϕ_c. This phenomenon has also been reported previously with polymer stabilized large particles in low MW solvent.[35] We report viscosities based on average shear stress and shear rate. If there are flow instabilities or shear banding, we did not observe them.

Shear thinning in dilute colloidal suspensions occurs as hydrodynamic forces alter suspension microstructure. These effects have been extensively studied with calculations of changes to microstructure with stress predicted and measured.[36] As volume fraction is raised, the suspension develops a glassy response where G'' develops a minimum. This behavior manifests itself in continuous shear as the slope p for the dynamic stress plateau decreasing rapidly as volume fraction is raised. The shear rate at which hydrodynamic forces dominate over thermodynamic forces is a weak function of volume fraction (i.e., Pe_2 shows a weak volume fraction dependence), and the range of shear rates where shear thinning is observed increases. These ideas have been developed for particles suspended in low molecular weight solvents but apply equally to the composite systems at hand.

The dynamic glass transition theory postulates that above a crossover volume fraction, ϕ_x, corporative motion is increasingly required for particles to exchange nearest neighbors. For $\phi_c/\phi_x < 1$, increases in shear stress result in continuous changes of suspension microstructure and shear thinning occurs by smooth and rapid diffusion. As ϕ_c/ϕ_x grows above unity, particles become increasingly localized, the barrier to diffusion increases rapidly, and the rate of diffusion decreases rapidly, resulting in a rapidly increasing zero shear rate viscosity. For $Pe_1 < Pe < Pe_2$, if the dynamical energy barrier height were independent of the applied stress, the result would be a dynamic yield stress plateau where the stress is independent of Pe ($\tau^* \sim Pe^p$ where $p \sim 0$).[37] In this region particles are trapped by nearest neighbors for a substantial period of time before the imposed microstructural deformation forces particles to rearrange their microstructure and energy is dissipated in rapid particle jumps at a rate that controlled by the thermodynamic forces acting on the particles and thus is independent of the applied shear rate.[37] If the applied stress is sufficient to alter suspension microstructure such that the energy dissipated in each particle jump decreases with increased shear rate, a weaker yield stress plateau will be observed ($p > 0$). The more strongly localized are the particles due to crowding or due to interparticle forces, the less the rate of deformation is controlled by smooth deformation and the larger the fraction of energy in the sheared system will be dissipated by rapid jumps between localized positions. The high shear rate terminal regime is entered at Pe_2 where the rate of deformation becomes comparable to the rate of diffusion over the dynamical barrier. For larger shear rates, a high shear rate plateau viscosity is achieved and hydrodynamic interactions control stress transfer and the suspension microstructure.[38] These hydrodynamic stresses ultimately drive particles to form hydroclusters, and at Pe_3, shear thickening is observed.

This idealized picture is altered by details of particle interactions as seen for the four sets of data shown in Figure 7 where we compare flow curves at the same volume fraction

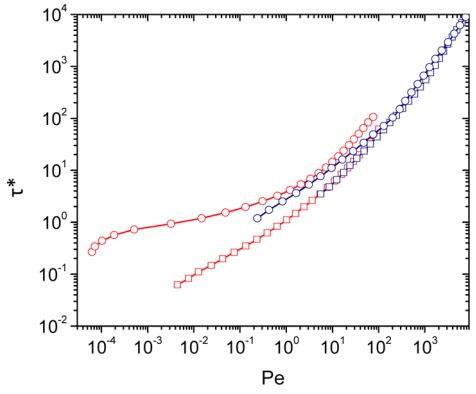

Figure 7. Flow curves for small particles (red) and large particles (blue) suspended in PEG 400 (square) and PEG 2000 (circle) at $\phi_c \sim 0.505$ (SCSP: 0.511; LCSP: 0.510; SCLP: 0.501; and LCLP: 0.504).

for the two particle sizes suspended each in the two polymer melts. The growth of p (i.e., the weakening of the dynamic yield stress plateau) and an increase in Pe_1 are associated with a decrease in R_g/D_c. At this volume fraction, the high shear rate viscosity is similar for all but the SCLP. This system displays a very slow approach to high shear rate terminal viscosity dominated purely by hydrodynamic interactions. If the particles behaved as hard spheres, the flow curves in Figure 7 would superimpose. This is seen for SCSP and LCSP samples over the range of Pe where we could gather overlapping data, suggesting the samples interact weakly. However, consistent with the linear and nonlinear viscoelastic data shown in previous sections increasing polymer molecular weight alters particle interactions at low shear rates indicating that the increased

dx.doi.org/10.1021/ma301184t | Macromolecules 2012, 45, 9791−9803

molecular weight alters the potentials of mean force experienced by the particles.

Here to explore the shear thinning behavior, we use the slope p at the inflection point Pe_d where $[(d^2 \log(\tau^*)]/[d \log(Pe)^2] = 0$ (or the stress plateau region where the slope $p = d \log(\tau^*)/d \log(Pe)$ is constant). p decreases with increasing volume fraction as expected, with the detailed information on p supplied in the Supporting Information. We did not present the values of p for LCSP as we are not able to get to measure stresses at sufficiently small values of Pe to track the inflection point. Based on other comparisons, similar behaviors between SCSP and LCSP are expected for the slope at the inflection point. Of particular significance is that at fixed $\phi_c \sim 0.505$ (as shown in Figure 7), p increases as R_g/D_c decreases, indicating that the development of a well-defined yield stress plateau is sensitive to soft interactions that are 1% or less of the particle diameter. This can be imagined as indicating that particles are more highly constrained by nearest neighbors and that the barrier to flow is less readily degraded as the extent of the adsorbed polymer layer relative to the particle size increases. And when changing to PEG2000, p decreases sharply especially for SCLP.

As pointed by de Kruif et al.,[36] the viscosity of hard-sphere systems at shear-thinning region correlates empirically with

$$\frac{\eta_r - \eta_{r,\infty}}{\eta_{r,0} - \eta_{r,\infty}} = \frac{1}{1 + (\tau^*/\tau_d)^m} \quad (2)$$

Here $\eta_{r,0}$ is the relative zero shear viscosity of the suspension, $\eta_{r,\infty}$ is the relative high shear rate viscosity of the suspension, τ_d is the critical dimensionless shear stress which can be treated as the inflection point of the stress plateau and is a function of volume fraction, and m is a fitting parameter. This correlation works well up to $\phi_c \sim 0.50$ for hard sphere systems with $1.4 < m < 1.8$. At elevated volume fraction where $\eta_{r,\infty} \ll \eta_{r,0}$, $p = 2/(2 + m)$ yielding for volume exclusion and weakly attractive systems below the gel point[2,39−41] $0.53 < p < 0.59$. By assuming that this correlation characterizes the ability of shear to alter microstructure and stress transfer at volume fractions where the particles are not localized, we are able to define a glass or gel volume fraction as that point where $p < 0.56$. Using this definition, we see that the gel or glass transition occurs at volume fractions of 0.511, 0.330, and 0.549 for SCSP, SCLP, and LCLP, respectively. We note that p changes in a continuous manner as volume fraction is raised and that this definition of kinetic arrest is somewhat arbitrary. On the other hand, the volume fractions of kinetic arrest defined by this method are close to those where ω_m is first observed: corresponding to 0.533, 0.369, and 0.570 for SCSP, SCLP, and LCLP, respectively, indicating a variety of measures capture the onset of rapid slowing of relaxation times with increasing volume fraction.

Shear thickening is associated with hydrodynamic stresses forcing particle together and the buildup of clusters held together by shear forces. At high volume fraction these clusters span the shear gap and result in positive normal stresses and discontinuous jumps in viscosity as shear rate is increased. Shear thickening is delayed by strong interparticle forces—attractions or repulsions. The larger the repulsion is, the higher the shear rate is required to establish the correct hydrodynamic conditions to drive cluster formation. As shown in Figure 6, SCSP, LCLP, and LCLP all reach hydrodynamically controlled stress transfer and shear thickening is observed. For the SCLP case, the interparticle forces remain sufficiently strong that, over the shear stress range probed, hydrodynamic forces cannot overcome interparticle forces and thickening is not observed. The dimensionless stresses at the onset of thickening are shown in Figure 8A with detailed values shown in the Supporting Information. While hydrodynamic forces must dominate stress transfer to observe shear thickening, short-range interparticle forces also are known to have a strong impact on the shear rate at the onset and the degree of shear thickening. For particles only experiencing excluded volume interactions, due to the no flux boundary condition at the particle−fluid interface, Brownian forces gives rise to large gradients in particle number density at the particle surface. The pair distribution function relates hydrodynamic and Brownian forces through the conservation equation and equation governing particle motion. The gradient of pair distribution function is a measure of the effect of magnitude of the thermodynamic force required to balance hydrodynamic force and ensure the no-flux boundary condition. For hard spheres the critical stress at thickening scales as D_c^{-3}. As discussed below, the composites studied here do not display this size scaling, and we are forced to recognize that even for the low molecular weight polymer, the details of the potential of mean force near contact are important in establishing the onset and magnitude of the thickening.[8]

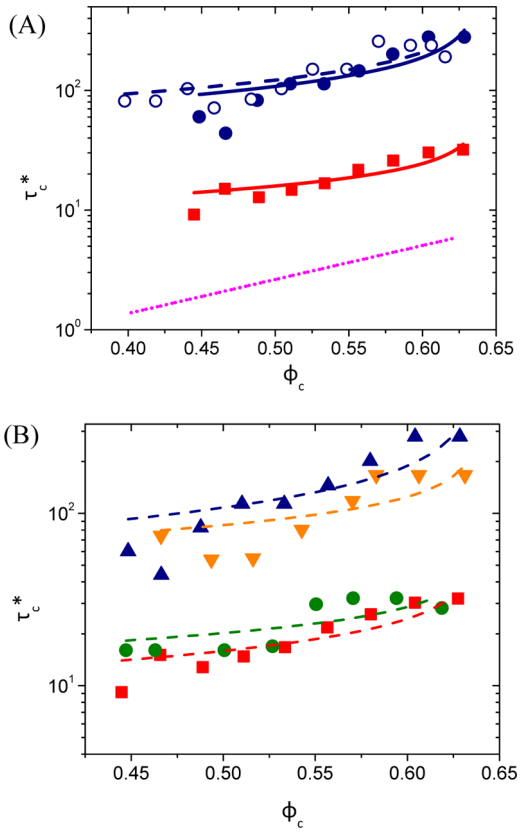

Figure 8. (A) Dimensionless shear stress for onset thickening for SCSP (■), LCSP (●), and LCLP (○) plot as a function of volume fraction. The solid line (red for SCSP, blue for LCSP) and dashed line (LCLP) are fitting curves in form of eq 6. The dotted line is the correlation of hard sphere experiment experiencing Brownian force reported before.[16] (B) Dimensionless shear stress for onset thickening for particles in PEG400 D_c = 127 nm (■), D_c = 213 nm (●), D_c = 612 nm (▲), and D_c = 730 nm (▼) plot as a function of volume fraction. The dashed line is fitting curve in form of eq 6.

dx.doi.org/10.1021/ma301184t | Macromolecules 2012, 45, 9791−9803

We observe that the stress at thickening is a weakly increasing function of volume fraction. We associate this with the average interparticle spacing such that as the particles approach contact, the stress required for them to thicken will diverge. The equilibrium surface separation, h, can be expressed as

$$h/D_c = (\phi_m/\phi_c)^{1/3} - 1 \quad (3)$$

As the adsorbed polymer layer soft interaction is important, proved already in dilute suspension, here we would incorporate a simplified surface interaction potential in the following form:[16]

$$U(r) = Ah^{-B} \quad (4)$$

where A and B are fitting parameters determined by polymer size and particle size. Here we base our discussion on the assumption of force balance where hydrodynamic force equals potential of mean force at the equilibrium surface separation.

$$\frac{3\pi\tau_c D_c^3}{16h} = -k_B T \frac{\partial(U/k_B T)}{\partial r} \quad (5)$$

From these expressions we postulate that interparticle forces influence the stress scale but not the volume fraction dependency of this divergence and write the dimensionless stress at thickening as

$$\tau_c^* = C\left[\left(\frac{\phi_m}{\phi_c}\right)^{1/3} - 1\right]^{-B} \quad (6)$$

where ϕ_m is a maximum packing fraction (set here to be 0.64 consistent with previous experimental studies[36]). We anticipate C will be independent of volume fraction and carry information about particle size and pair potential while B will be a universal constant. Shown in Figure 8A,B are plots of τ_c^* fit with eq 6. We tabulate best fits for our data in Table 3 where we note our expectation of a constant value of the exponent B within experimental uncertainty. Our experimental results of critical shear stresses for small particles in PEG400 and large particles in PEG400 and PEG2000 are summarized in Supporting Information and presented in Figure 8A along with a comparison of a previous correlation of experimental data for hard spheres:[8]

Table 3. Fitting Parameters of Eq 6 for Particles Suspended in PEG400 and LCLP

particle size D_c (nm)	D_c/R_g	B	C
127 (PEG400)	158	0.31 ± 0.06	7.3 ± 1.6
213 (PEG400)	266	0.26 ± 0.10	10.8 ± 3.8
612 (PEG400)	765	0.41 ± 0.08	39.8 ± 13.6
730 (PEG400)	912	0.28 ± 0.09	43.5 ± 16.3
612 (PEG2000)	322	0.39 ± 0.09	46.7 ± 15.2

$$\frac{\tau_c D_c^3}{8k_B T} = 0.1e^{\phi/0.153} \quad (7)$$

The proposed scaling captures the data well with B a weak function of D_c or R_g and the coefficient C dependent on D_c. Here C increases with D_c in PEG400, showing a scaling $\tau_c \propto D_c^{-\alpha}$ where α is smaller than 3. The change in modulus with polymer molecular weight is associated with an increase in attraction which is expected to delay thickening. This expectation is confirmed with magnitude of τ_c^* being slightly larger for LCLP than LCSP.[13] Previous studies with silica particles dispersed in silicon oil have shown that medium viscosity has no effect on critical shear thickening stresses. In these studies a universal shear response is observed when hard sphere scaling and effective volume fractions are used. As a result, we can conclude that deviations from this universal behavior result from variations in particle interactions.[42] Similarly in our study where the viscosity kept constant with temperature increasing for LCLP, we do not attribute the slight increasing observed in τ_c^* to the temperature change which affects the dimensionless scaling, but to an increased attractive interaction that results from increasing polymer MW. This conclusion is confirmed by the disappearance of shear thickening when moving from SCSP to SCLP.

To confirm the particle size scaling of thickening in PEG400 melts, we gathered thickening data on two more particle size (D_c = 213 nm and D_c = 730 nm). The critical stresses at the onset of thickening are shown Figure 8B with the results of fitting the data summarized in Table 3. In Figure 9, we show how the characteristic critical stress for thickening varies as a function of D_c/R_g, where R_g is held constant and D_c is varied. C increases from near zero for small D_c/R_g according to a linear manner and approaches a constant value at large D_c/R_g, which can be explained as a consequence of reduced particle softness when increasing D_c considering the thickness of polymer layer is constant. For these systems we expect the adsorbed polymer to reach equilibrium with polymer in the bulk and to result in a polymer layer of thickness ~1 nm.[2] The particles are thermodynamically stable and the potential of mean force is short-range and monotonically repulsive. The results in Figure 9 indicate that only for $D_c/R_g > 600$ with the influence of that soft repulsion begin to have minimal influence on the onset of thickening. Therefore, under conditions of small D_c ($D_c/R_g <$ 600), the soft interactions of the adsorbed layers drive the critical stress to scale as $\tau_c \propto D_c^{-2}$ instead of $\tau_c \propto D_c^{-3}$, even though hard sphere behavior is seen in the low shear rate viscosity under dilute conditions. This may be explained as a consequence of adsorbed polymer layer deformation when applying high shear. A similar mechanism has been applied to explain the shear thinning behavior for smaller particles.[43] In addition, we note that the ω dependence of G' at high frequencies also reflects the deformation of polymer layers. As

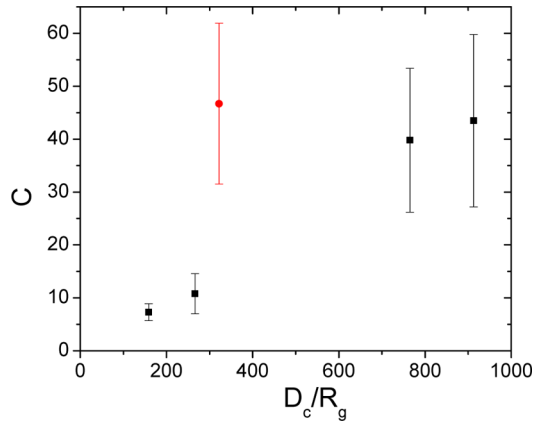

Figure 9. Coefficient of eq 6 C as a function of D_c/R_g for particles dispersed in PEG 400 (■) and in PEG 2000 (●).

dx.doi.org/10.1021/ma301184t | Macromolecules 2012, 45, 9791−9803

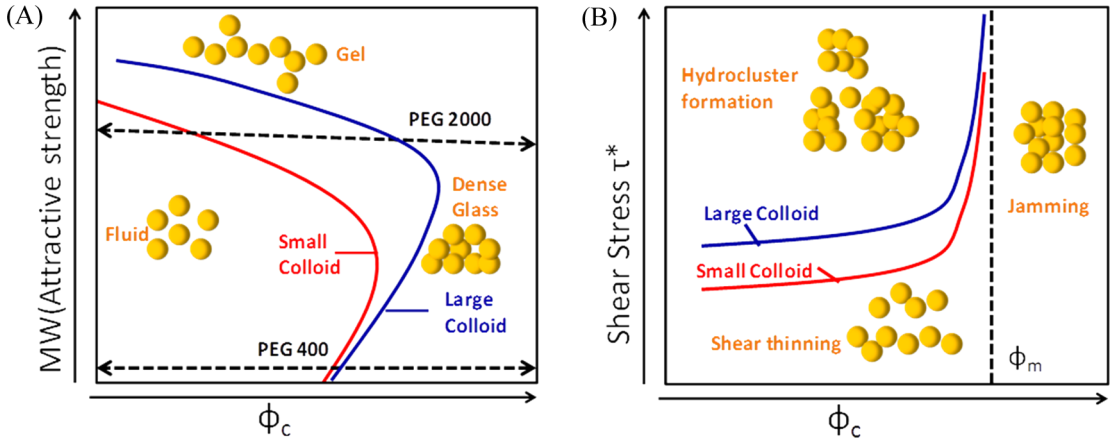

Figure 10. (A) Schematic dynamical arrest transition boundaries in the panel of polymer MW−ϕ_c for different particle sizes. (B) Schematic shear thickening boundaries in the panel of τ^*−ϕ_c for different particle sizes in PEG400.

the particles are thermodynamically dispersed in polymer melts, no irreversible aggregation is observed in the high shear response. However, we note that with increased molecular weight, the attractions produced by having the polymer adsorb in a nonequilibrium manner increase the critical stress for thickening.

E. The Role of Polymer-Induced Particle−Particle Interaction in Controlling Viscoelasticity of Composites. Four different sets of colloid−polymer composites are designed purposely here to understand the role of polymer induced particle−particle interaction in controlling composite viscoelasticity. Specifically, particles are suspended in PEG400 and PEG2000. These polymers molecular weights are chosen as they remain under the entanglement limit but are sufficiently different to alter pair interaction potentials. Two different particle sizes are chosen, where D_c = 612 nm for large particles and D_c =127 nm for small particles, to provide a measure of the effects of changes in particle size on characteristic shear stresses, shear rates, and strain frequencies.

From linear rheology where we investigate the samples at a strain frequency in the elastic modulus plateau and flow curves where we investigate properties at shear rates in the dynamic stress plateau, we conclude that by changing the suspended medium from PEG400 to PEG2000 attractive interactions are introduced. Our studies suggest that with increasing volume fraction the SCLP enters dynamical arrest state. This occurs at a value of ϕ_c, suggesting formation of strongly bonded gel. The LCLP system shows a much higher dynamical arrest transition volume fraction lying close to the value of LCSP. Considering all these effects, we propose a state diagram showing dynamical arrest transition boundaries in Figure 10A in the panel of polymer MW−ϕ_c. In low-MW polymers (PEG400), particles experience basically volume exclusive interaction and both particles form dense glasses at large ϕ_c. For high-MW polymers (PEG2000), the interparticle attractions are introduced with strength and range independent of particle size. For LCLP, attractive dense glasses are formed showing dynamical arrest transition volume fraction close to that seen with the LCSP system. This is attributed to re-entrant behavior.[44] For SCLP, the relative attractive range (scaled with particle size) is larger, this re-entrant behavior is suppressed, and a gel is formed at low ϕ_c. This suppression of re-entrant behavior due to attraction range enlarge has been predicted.[45]

To understand the polymer-induced soft interaction in PEG400, it is necessary to apply high shear rate and study shear thickening phenomenon. In Figure 10B, we propose a state diagram of shear thickening in the panel of τ^*−ϕ_c. For a fixed particle size, at for τ^* just below τ_c^*, shear thinning occurs. When crossing the boundary of τ_c^*, hydroclusters are formed with shear thickening observed. τ_c^* is a weak function of ϕ_c but increases sharply when approaching maximum packing fraction ϕ_m, where jamming conditions can be achieved. This shear thickening transition boundary is moved to larger stresses by increasing D_c as a result of reducing the relative softness of the pair potential as characterized by a reduction of R_g/D_c, and saturation in reduced softness is observed for D_c/R_g > 600 as suggested in Figure 8B.

IV. CONCLUSION

These studies uncover a surprisingly complex set of phenomena associated with suspending particles in polymer melts. The system chosen has seen extensive study where we know the polymer segments have a strong affinity for the particle surface and that to high volume fractions the polymer remains adsorbed to the particle surface with a layer thickness growing approximately as R_g. This type of absorption is not predicted from equilibrium theories which are, however, able to capture polymer and particle microstructure at the lowest molecular weight, suggesting nonequilibrium absorption for higher molecular weight polymers. We associate this nonequilibrium absorption with an increase in interparticle attraction and suggest this is due to a depletion effect where polymer segments in the bulk observe a particle surface that appears as if it is composed of polymer segments instead of the bare silica as experienced when the polymer segments can easily equilibrate with those in the bulk.

The consequences of these polymer particle interactions are seen in dense suspension rheology where for low molecular weight (PEG400) the particles appear to interact as expected for particles experiencing short-range repulsive interactions. The composites undergo glass transitions with a cross over volume fraction near 0.5 where a separation of relaxation times becomes apparent indicating the onset of caging. The softness of the repulsive interaction is, however, important at high stresses where the onset of thickening is delayed to higher stresses as D_c/R_g increases with an apparent saturation for D_c/R_g > 600.

In the high molecular weight polymer we see evidence of attractions. For the small particles, the attractions are sufficient to produce a gel at volume fractions above 0.3 while for the large particles the attractions effect is not large enough to shift the suspensions to gelation. The attractions are of sufficient magnitude that thickening is not observed for small particles.

One surprising result of this study is the substantial rheological consequences in moving from a polymer with degree of polymerization of 9 to a polymer with degree of polymerization of 45. Both degrees of polymerization are below the entanglement value of ∼100−150. Thus, the adsorption of the polymer to the particle surface induces interactions that are not at equilibrium well below the point where the polymers entangle and these nonequilibrium effects have substantial rheological consequences. Particles are often added to polymer melts to enhance composite elasticity. Often this is attributed to particle induced polymer interactions (e.g., the particles alter polymer relaxation times by creating effective cross-link points). Here we show that substantial alterations to composite properties can arise where the particles are, on average, spaced at many times the polymer radius of gyration due to polymer induced changes to particle interactions.

■ ASSOCIATED CONTENT

Supporting Information

Table S1, showing characteristic rheology parameters for different composites under continuous shear. This material is available free of charge via the Internet at http://pubs.acs.org.

■ AUTHOR INFORMATION

Corresponding Author

*E-mail czukoski@illinois.edu.

Notes

The authors declare no competing financial interest.

■ ACKNOWLEDGMENTS

This material is based on work supported by the U.S. Department of Energy, Division of Materials Science, under Award DE-FG02-07ER46471, through the Frederick Seitz Materials Research Laboratory at the University of Illinois Urbana−Champaign. Research in this work was carried out in part in the Frederick Seitz Materials Research Laboratory Central Facilities, University of Illinois University, which are partially supported by the U.S. Department of Energy under Grants DE-FG02-07ER46453 and DE-FG02-07ER46471.

■ REFERENCES

(1) Koo, J. H. *Polymer Nanocomposites: Processing, Characterization, and Applications*; McGraw-Hill: New York, 2006.
(2) Anderson, B. J.; Zukoski, C. F. *Macromolecules* **2008**, *41*, 9326−9334.
(3) Tuteja, A.; Mackay, M. E.; Narayanan, S.; Asokan, S.; Wong, M. S. *Nano Lett.* **2007**, *7*, 1276−1281.
(4) Anderson, B. J.; Zukoski, C. F. *J. Phys.: Condens. Matter* **2009**, *21*, 285102.
(5) Granick, S.; Hu, H. W. *Langmuir* **1994**, *10*, 3857−3866.
(6) Hu, H. W.; Granick, S. *Science* **1992**, *258*, 1339−1342.
(7) Maranzano, B. J.; Wagner, N. J. *J. Chem. Phys.* **2001**, *114*, 10514−10527.
(8) Maranzano, B. J.; Wagner, N. J. *J. Rheol.* **2001**, *45*, 1205−1222.
(9) Anderson, B. J.; Zukoski, C. F. *Langmuir* **2010**, *26*, 8709−8720.
(10) Schweizer, K. S.; Curro, J. G. *At. Model. Phys. Prop.* **1994**, *116*, 319−377.
(11) Hall, L. M.; Anderson, B. J.; Zukoski, C. F.; Shweizer, K. S. *Macromolecules* **2009**, *42*, 8435−8442.
(12) Kim, S. Y.; Hall, L. M.; Schweizer, K. S.; Zukoski, C. F. *Macromolecules* **2010**, *43*, 10123−10131.
(13) Kim, S. Y. University of Illinois Urbana−Champaign, 2011.
(14) Anderson, B. J.; Zukoski, C. F. *Macromolecules* **2009**, *42*, 8370−8384.
(15) Buscall, R.; Ettelaie, R. *Ind. Eng. Chem. Res.* **2006**, *45*, 6915−6922.
(16) Krishnamurthy, L. N.; Wagner, N. J.; Mewis, J. *J. Rheol.* **2005**, *49*, 1347−1360.
(17) Siebenburger, M.; Fuchs, M.; Winter, H. H.; Ballauff, M. *J. Rheol.* **2009**, *53*, 707−726.
(18) Lu, Y.; Ballauff, M. *Prog. Polym. Sci.* **2011**, *36*, 767−792.
(19) Dingenouts, N.; Norhausen, C.; Ballauff, M. *Macromolecules* **1998**, *31*, 8912−8917.
(20) Senff, H.; Richtering, W.; Norhausen, C.; Weiss, A.; Ballauff, M. *Langmuir* **1999**, *15*, 102−106.
(21) Larson, R. G. In *Topics in Chemical Engineering*; Gubbins, K., Ed.; Oxford University: New York, 1999; pp 342−353.
(22) Wagner, N. J.; Brady, J. F. *Phys. Today* **2009**, *62*, 27−32.
(23) Gopalakrishnan, V.; Zukoski, C. F. *J. Rheol.* **2004**, *48*, 1321−1344.
(24) Stober, W.; Fink, A.; Bohn, E. *J. Colloid Interface Sci.* **1968**, *26*, 62−&.
(25) Bogush, G. H.; Tracy, M. A.; Zukoski, C. F. *J. Non-Cryst. Solids* **1988**, *104*, 95−106.
(26) Batchelor, G. K. *J. Fluid Mech.* **1977**, *83*, 97−117.
(27) Mewis, J.; Wagner, N. J. *Colloidal Suspension Rheology*; Cambridge University Press: Cambridge, UK, 2012.
(28) Helgeson, M. E.; Wagner, N. J.; Vlassopoulos, D. *J. Rheol.* **2007**, *51*, 297−316.
(29) Mason, T. G.; Weitz, D. A. *Phys. Rev. Lett.* **1995**, *75*, 2770−2773.
(30) Kobelev, V.; Schweizer, K. S. *Phys. Rev. E* **2005**, *71*, 021401.
(31) Schweizer, K. S.; Yatsenko, G. *J. Chem. Phys.* **2007**, *127*, 164505.
(32) Chen, Y. L.; Schweizer, K. S. *J. Chem. Phys.* **2004**, *120*, 7212−7222.
(33) Lionberger, R. A.; Russel, W. B. *J. Rheol.* **1994**, *38*, 1885−1908.
(34) Hooper, J. B.; Schweizer, K. S. *Macromolecules* **2006**, *39*, 5133−5142.
(35) Larsen, R. J.; Kim, J. W.; Zukoski, C. F.; Weitz, D. A. *Phys. Rev. E* **2010**, *81*, 011502.
(36) Dekruif, C. G.; Vanlersel, E. M. F.; Vrij, A.; Russel, W. B. *J. Chem. Phys.* **1985**, *83*, 4717−4725.
(37) Bonnecaze, R. T.; Brady, J. F. *J. Rheol.* **1992**, *36*, 73−115.
(38) Russel, W. B.; Saville, D. A.; Schowalter, W. R. *Colloidal Dispersions*; Cambridge University Press: Cambridge, UK, 1989.
(39) Rodriguez, B. E.; Kaler, E. W.; Wolfe, M. S. *Langmuir* **1992**, *8*, 2382−2389.
(40) Mewis, J.; Frith, W. J.; Strivens, T. A.; Russel, W. B. *AIChE J.* **1989**, *35*, 415−422.
(41) Rueb, C. J.; Zukoski, C. F. *J. Rheol.* **1998**, *42*, 1451−1476.
(42) Shenoy, S. S.; Wagner, N. J. *Rheol. Acta* **2005**, *44*, 360−371.
(43) Sarvestani, A. S. *Nanoscale Res. Lett.* **2010**, *5*, 791−794.
(44) Dawson, K.; Foffi, G.; Fuchs, M.; Gotze, W.; Sciortino, F.; Sperl, M.; Tartaglia, P.; Voigtmann, T.; Zaccarelli, E. *Phys. Rev. E* **2001**, *63*, 17.
(45) Tripathy, M.; Schweizer, K. S. *Phys. Rev. E* **2011**, *83*, 041406.